



Universiteit
Leiden
The Netherlands

Temperature and pressure effects on the electrochemical CO₂ reduction

Vos, R.E.

Citation

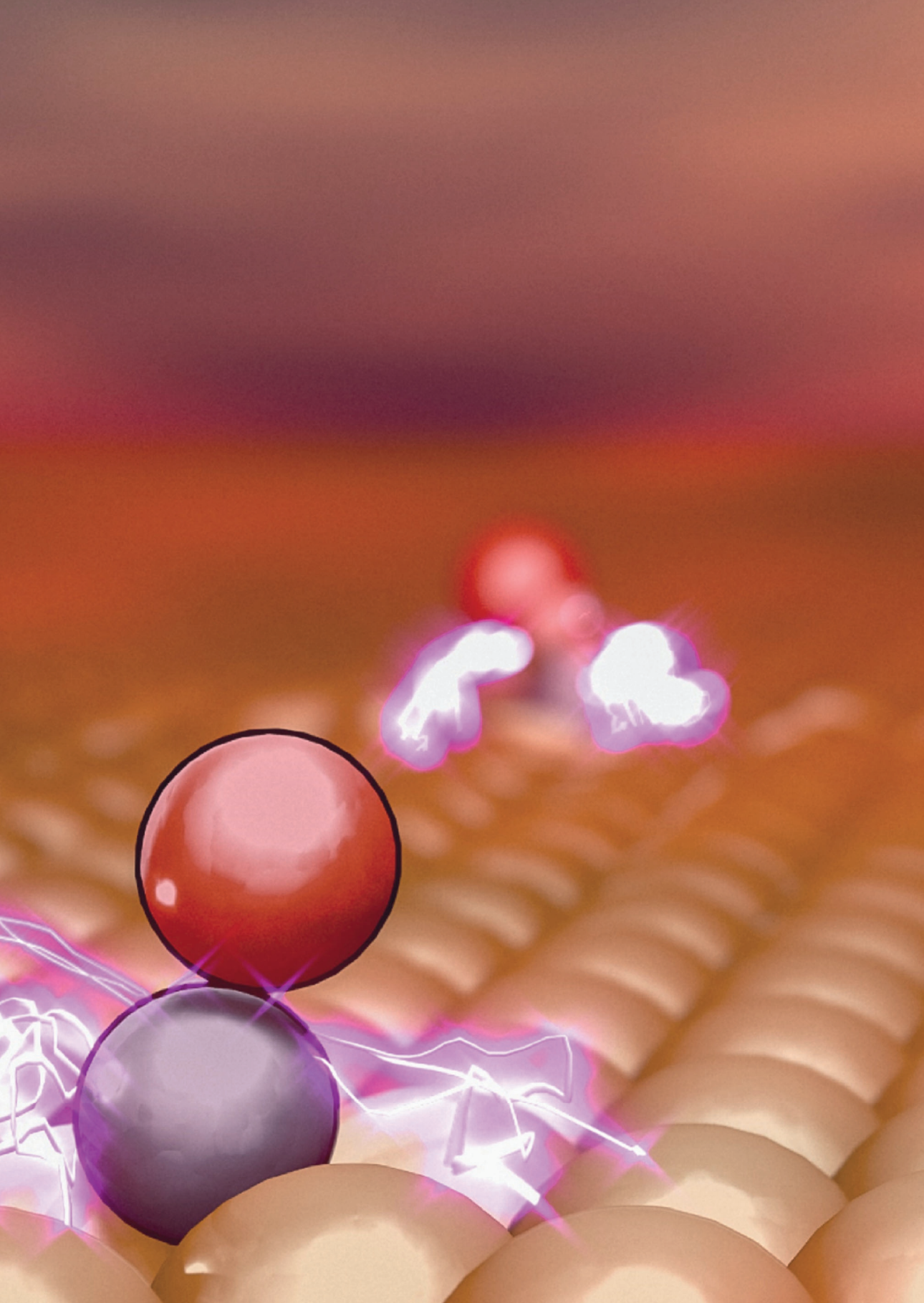
Vos, R. E. (2025, February 5). *Temperature and pressure effects on the electrochemical CO₂ reduction*. Retrieved from <https://hdl.handle.net/1887/4179004>

Version: Publisher's Version

License: [Licence agreement concerning inclusion of doctoral thesis in the Institutional Repository of the University of Leiden](#)

Downloaded from: <https://hdl.handle.net/1887/4179004>

Note: To cite this publication please use the final published version (if applicable).



4

The temperature dependence of electrochemical CO₂ reduction on Ag and CuAg alloys

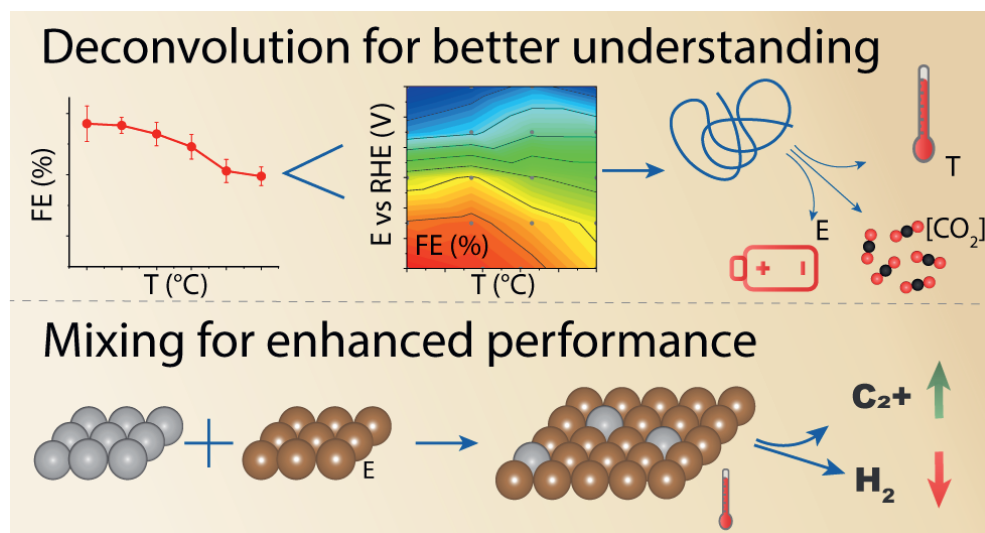
This chapter is based on R.E. Vos, J.S. Smaak, M.T.M. Koper *Journal of Catalysis* 115613 (2024)

4. The temperature dependence of electrochemical CO₂ reduction on Ag and CuAg alloys

Abstract:

Ag is often studied as catalyst for electrochemical CO₂ reduction as it shows high selectivity towards CO and is easily alloyed with Cu to enhance performance using CuAg catalysts. In this study, we investigated the effect of temperature on Ag and CuAg catalysts and compare these with previous results on Au and Cu catalysts. We show that the temperature effect is complicated as it shows an interplay with CO₂ concentration, potential and mass transport. It is therefore crucial to deconvolute these parameters and study the effect of temperature under different conditions. Moreover, we show that alloying Ag with Cu can inhibit some of the deactivation effects observed at high temperatures on pure Cu. CuAg alloys can prevent the dominance of hydrogen evolution at elevated temperatures, although an optimum of C₂⁺ products with temperature is still observed.

4



4.1 Introduction

Electrochemical CO₂ reduction has the potential to recycle CO₂ and be used in a sustainable and clean economy.^{1,2} Copper is often studied as a catalyst for CO₂RR as it can produce multicarbon products such as ethylene and ethanol. Au and Ag are also frequently studied catalysts as they are (model) catalysts producing mainly CO and H₂. They are known to be among the most active and selective catalysts towards CO.³⁻⁸ This high selectivity is due to the weak hydrogen and CO binding strength on these metals, which avoids further reduction of CO or CO poisoning, while also suppressing the hydrogen evolution reaction (HER).^{9,10}

Ag produces mostly CO or H₂ depending on the potential. The optimum selectivity towards CO is reached around -1.1 V vs RHE.³ With increasing overpotential, Ag can also produce quite some HCOOH. Moreover, at very high overpotentials it has been shown to produce methane, methanol and ethanol.³ At ambient pressure this was maximum -0.01 mA/cm²,³ but at elevated pressures these activities are increased considerably.¹¹ Moreover, at elevated pressures, other multicarbon products such as acetic acid, ethylene glycol and n-propanol can also be produced, showing that Ag is capable of making C-C bonds, provided that the experimental conditions promote higher CO coverages.¹¹

Recently, more studies have looked at the effect of temperature on the electrochemical CO₂ reduction, as temperature is an understudied but relevant parameter. Au, as a simple model catalyst, shows a beneficial effect with regard to the Faradaic efficiency (FE) towards CO with increasing temperature up to 55 °C.¹² On Ag in a gas-diffusion electrode (GDE) system, an optimum in FE with temperature has been observed as well, although only 3 temperatures were studied.¹³ It is interesting to study in more detail if the temperature effect on Ag is similar to that found before on Au and if Ag is able to make C-C bonds at elevated temperatures. On copper, increasing temperature also results in an optimum, both in CO₂RR activity and in C₂⁺ selectivity.¹⁴ The decrease in both activity and selectivity at high temperatures is due to the dominance of HER under these conditions. This behaviour was tentatively related to a change in the copper surface, combined with a too high local pH. Alloying of Cu might be a strategy to prevent the change in the Cu surface and inhibit HER at higher temperatures.

Ag is one of the metals used to alloy with Cu to obtain higher efficiencies towards C₂⁺ products,¹⁵⁻²⁰ and might be interesting to inhibit HER at elevated temperatures as it has shown this capability at ambient temperature.²⁰⁻²² The underlying idea of combining Cu with Ag is that in this catalyst, Ag will produce the CO, which can spill over to the Cu to give higher CO coverages and higher C₂⁺ efficiencies.²¹⁻²⁶ However, some studies show that the effect of alloying is more a

strain effect than a spillover effect.^{17,21} Moreover, the composition of the surface alters the d-band center which could tune the *CO binding strength, thus controlling the product selectivity.¹⁶ The exact composition of the (surface) alloy has been shown to alter the selectivity significantly.^{16,20} There are reports of CuAg alloys with a FE of above 60% towards CH₄,^{18,27} although most studies indeed report increased selectivity towards C₂+ products, specifically oxygenates.^{15,19,21} For example, FEs towards acetaldehyde of 70%,¹⁵ or ethanol with more than 35% FE, have been reported.²⁸

In this chapter, we show that temperature has an important effect on the electrochemical CO₂ reduction on Ag, but this effect is not similar at all applied potentials. This is due to the significant dependence of CO₂RR on Ag on the bulk CO₂ concentration and mass transport. This interdependence illustrates that other parameters have to be taken into account to make proper conclusions about the effect of a single parameter such as temperature. We also show that the exact nature of the CuAg electrode can result in very different product distributions. Nonetheless, in all cases there is an optimum in C₂+ products at a temperature around 40 °C, just as on bare Cu. However, with the right alloy we observe that it is possible to reduce the dominance of HER at higher temperature and maintain significant FE for CO₂ reduction.

4.2 Experimental

4.2.1 Chemicals

AgNO₃ (Acros Organics) was used for the galvanic exchange. The electrolytes for electrolysis was prepared from KHCO₃ (99.95%, Sigma-Aldrich), CsHCO₃ (99.99%, Alfa Aesar) and Milli-Q water (≥ 18.2 M Ω cm, TOC < 5 ppb). The electrolytes were stored with Chelex (100 sodium form, Sigma-Aldrich) to clean the electrolyte from any metal impurities.²⁹ Ar (5.0 purity, Linde) and CO₂ (4.5 purity, Linde) were used for purging the electrolytes.

4.2.2 General Electrochemical Methods

The experiments were performed in a home-made PEEK H-cell. To clean the cell prior to experiment, all parts were stored overnight in permanganate solution (0.2 M H₂SO₄, 1g/L KMnO₄). Before use, the cell was rinsed, washed in diluted piranha to remove any traces of MnO₄ and MnO₂, rinsed again and boiled three times with Milli-Q water. A three-electrode configuration was used during experiments. The reference electrode was a commercial RHE (mini Hydroflex, Gaskatel) and was placed in the same compartment as the working electrode. The counter electrode was a dimensionally stable anode (DSA, Magneto) and was

separated from the working electrode by an anion exchange membrane (AMVN Selemion, AGC). All the electrochemical measurements were carried out using an IviumStat potentiostat (Ivium Technologies). The flow of CO₂ (and Ar for the partial pressure experiments) was controlled using a mass flow controller (SLA5850, Brooks Instrument).

4.2.3 Electrode preparations

The polycrystalline Ag working electrode (99.99%, Mateck) was mechanically polished with decreasing diamond polishing suspension (3.0, 1.0 and 0.25 μm, Buehler) on micropolishing cloths (8 in.) until the surface was mirror polished. Then, the electrode was successively sonicated in ethanol and Milli-Q water for 3 min to remove any impurities and dried with pressurised air, after which the electrode was ready to use.

A polycrystalline Cu working electrode (99.99%, Mateck) was used for the CuAg experiments. First, the electrode was mechanically polished similar as described above for the Ag electrode. After mechanical polishing, the Cu disk was electrochemically polished in a solution of H₃PO₄ (85%, Suprapure, Merck) by applying +3 V versus a graphite counter electrode for 20 seconds and subsequently rinsed with Milli-Q water. A galvanic exchange method based on the work of Clark et al.²¹ was used to synthesize the CuAg surface alloy. Using a meniscus configuration, the electrode surface was put in contact with a AgNO₃ solution, which was heated to 50 °C. Different concentrations of AgNO₃ were used and either Ar was bubbled through the galvanic exchange solution or the solution was open to air. These different conditions were used as it was found they influence the product distribution after galvanic exchange. After 5 min the electrode was rinsed, dried with pressurized air and ready to use for the electrolysis experiments.

4.2.4 Electrolysis experiments

The electrolysis experiments were performed in a home-made PEEK H-cell containing 6.8 mL 0.1 M bicarbonate electrolyte in each compartment. Pictures and schematics of the jacketed cell can be found in Figures C.1 and C.2. For the experiments with Ag, KHCO₃ was used as electrolyte as this is common electrolyte for CO₂ reduction to CO. For the experiments with CuAg, CsHCO₃ was used to enhance the formation of multicarbon products and to increase the chances of gaining insights into the effect of temperature on minor CO₂RR products such as acetate and propionaldehyde. The PEEK H-cell was embedded in a home-made jacket which was connected to the water bath (Ecoline e100, Lauda) to control the temperature in the cell.¹⁴ Before electrolysis, CO₂ was purged through the electrolyte for 15 min while controlling the potential at -0.1 V vs RHE to saturate

4. The temperature dependence of electrochemical CO₂ reduction on Ag and CuAg alloys

the electrolyte and heat the electrolyte to the proper temperature. Then the ohmic drop was determined by electrochemical impedance spectroscopy (EIS) at -0.1 V vs RHE and 85% ohmic drop compensation was performed for all chronoamperometry measurements. Chronoamperometry was performed for either 60 min for the CuAg electrodes and for 32 min for the Ag electrodes. CO₂ was constantly purged at 20 mL/min during the experiments. At 5, 19, 32, 46 and 60 min a gas sample was online analyzed using a Shimadzu 2014 gas chromatograph containing two detectors (one TCD with a Shincarbon column and one FID with a RTX-1 column). A liquid sample was taken at the end of the electrolysis. The liquid products were analyzed using high performance liquid chromatography (HPLC, Shimadzu) with a Aminex HPX-87H column (Bio-rad).

4.2.5 Efficiency calculations

To be able to better compare the results on pure Cu with the results obtained with the CuAg alloys we have defined a Carbon efficiency as in a previous study.¹⁴ The Carbon efficiency is defined equivalently to the Faradaic efficiency:

$$CE = \frac{c_i * a_i}{\sum_i c_i * a_i} = \frac{c_i * \frac{j_i}{n_i}}{\sum_i c_i * \frac{j_i}{n_i}} \quad (4.1)$$

where c number of carbons in product i , a is the production rate in mol/min, j is the partial current density and n is the number of electrons transferred during CO₂RR, all for product i .

4.2.6 Partial pressure experiments

With the use of flow controllers the partial pressure of CO₂ can be altered by mixing the inlet flow with Ar gas. This allows us to change the CO₂ concentration in the bulk electrolyte independently of temperature. We estimate the CO₂ concentration using Henry's law in combination with an empirical equation to estimate Henry's constant.³⁰

$$c = KP \quad (4.2)$$

$$\log(K) = 108.3865 + 0.01985076 * T - \frac{6919.53}{T} - 40.4515 * \log(T) + \frac{669365}{T^2} \quad (4.3)$$

where c is the concentration, K is the Henry's constant, P is the partial pressure and T is temperature. Only for the partial pressure experiments, the CO₂

concentration is actively controlled. In other experiments it follows the temperature dependence of equation 4.3. So unless otherwise stated, the partial pressure of CO₂ is 1 bar.

4.2.7 Characterization of morphology and chemical composition

The electrochemical surface area (ECSA) was determined from the double layer capacitance measurements following the protocol of Morales et al.³¹ The potential was scanned in a broad potential range, namely -0.15 to 0.25 V vs. RHE at sufficiently high scan rates (200 – 1000 mV/s). The capacitance was determined from the current difference between the anodic and cathodic scan at 0.05 V vs. RHE plotted against the scan rate. The slope of this graph gives the double layer capacitance.

Micrographs of the CuAg electrodes were obtained by scanning electron microscopy (SEM) in an Apreo SEM (ThermoFisher Scientific) with an acceleration voltage of 10 kV and an electron beam current of 1.6 nA.

The XPS measurements were performed in a SPECS Phoibos system equipped with an XRM50 X-ray source set to the Al K-alpha line used along with a monochromator to excite the sample with a beam spot of 0.4 mm diameter at 55° incidence. The acceleration voltage was set to 12 kV and a power of 400 W was used for all the measurements. The HAS7500 hemispherical analyser with a pass energy of 20 eV was employed to analyse the photoemission. All peaks have been calibrated according to the Cu2p peak.³² All the atomic percentages were calculated according to the cross sections at the Al K-alpha energy.³³

To analyze the XPS data, CASA-XPS software was employed. For the peak fitting a Shirley background and a linear background were subtracted for the Ag3d and the Cu2p respectively. Gaussian-Lorentzian (50 curves) were used for peak fitting after using the respective background subtraction.

4.3 Results and discussion

4.3.1 Temperature effect on Ag

Figure 4.1 shows that the selectivity towards CO₂RR on Ag decreases with temperature. Interestingly, apart from a small increase at low temperatures, the partial current density towards CO is hardly effected by the temperature change and it is mostly the increase in HER which changes the selectivities. This is striking as this apparent independence of the CO₂RR activity on temperature is different from that observed on Au, Cu and Ni catalysts.^{12,14,34} Temperature not only

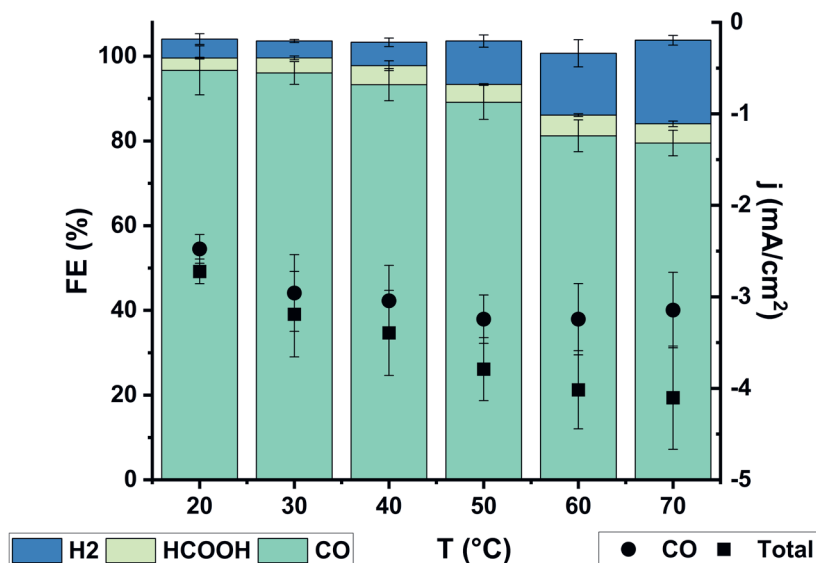


Figure 4.1 Temperature dependence of the Faradaic efficiency of CO₂RR on Ag at -1.1 V vs RHE in 0.1 M KHCO₃

influences the intrinsic kinetics of the reaction, but also influences many other parameters such as CO₂ solubility, pH and diffusion coefficients. Figure 4.1 shows the overall effect of temperature taking all these effects into account. The effect of the CO₂ concentration is convoluted with the intrinsic effect of temperature as the bulk concentration of CO₂ decreases with increasing temperature according to equation 4.3 as illustrated in Figure C.3. The different temperature dependences of the activity of Ag compared to the catalysts previously studied might be related to the strong dependence of the CO₂RR on Ag on the bulk concentration of CO₂.^{35,36} By changing the partial pressure of CO₂, the bulk concentration of CO₂ can be altered. From these partial pressure experiments we indeed observe a strong effect of the CO₂ concentration on the CO₂RR activity on Ag, as can be seen in Figure C.4.

To better understand the temperature dependence of Ag as observed in Figure 4.1, different potentials were studied as this might influence the temperature effect. Figure 4.2a shows that at a lower overpotential of -0.8 V vs RHE there is a strong dependence of the partial current density towards CO. The FE towards CO is only slightly affected by the temperature at this potential as also the current density for HER and for CO₂RR towards HCOOH increase with temperature. Additionally, for a

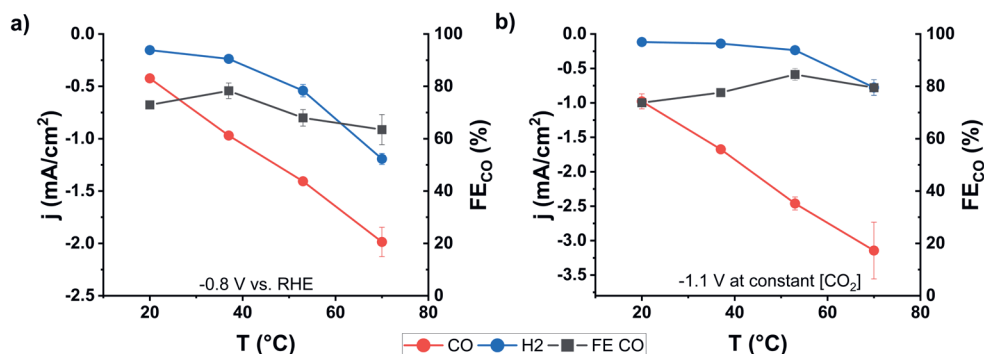


Figure 4.2 Temperature effect of the partial current densities for CO and H₂ and the FE for CO on Ag in 0.1 M KHCO₃ a) at -0.8 V vs RHE, and b) at constant CO₂ concentration by adjusting the partial pressure accordingly at -1.1 V vs RHE

better understanding of the overall effect of temperature on the CO₂RR on Ag, we try to deconvolute some of the effects of temperature. Some parameters change only slightly with temperature, such as pH,¹² or are difficult to deconvolute, such as the diffusion coefficient of CO₂. However, the parameter which is the most pronounced and easiest to deconvolute is the effect of temperature on the CO₂ bulk concentration. With increasing temperature the CO₂ solubility decreases as can be seen in Figure C.3. By adjusting the partial pressure accordingly, the bulk concentration can be maintained constant at different temperatures. This is primarily done to gain better understanding, and not for practical applications, as this means lowering the CO₂ concentration at the lower temperatures measured, which results in worse CO₂RR than at 1 bar of CO₂ partial pressure as illustrated in Figure C.4.

Figure 4.2b and C.5b show the effect of temperature at higher overpotential (-1.1V vs RHE) at a constant CO₂ concentration of 14 mM. This concentration is chosen as it is the concentration at the highest temperature of 70 °C at 1 bar of CO₂ partial pressure. Unlike in Figure 4.1, a strong dependence of CO₂RR activity with temperature can now be observed. Initially, the FE towards CO increases, but above 55 °C the efficiency slightly decreases. This indicates that the lack of temperature dependence in Figure 4.1 is due to the strong dependence of the CO₂RR on Ag on the bulk concentration. Figure C.5a shows that this also holds at a lower overpotential of -0.8 V vs RHE, where at constant CO₂ bulk concentration the partial current density towards CO as well as the corresponding FE increase even more strongly with temperature when the bulk CO₂ concentration is kept constant.

4

These results illustrate that even though understanding the overall temperature effect is imperative to link to (industrial) applications, it is important to deconvolute this overall effect in its single components to gain more insight into the exact nature of the temperature effect. Besides the direct effect of temperature on the kinetics, the effect on the bulk concentration of CO₂ is the most important factor to study. Moreover, to fully grasp the effect of a single parameter it is important to study this parameter at different conditions. For example, the effect of temperature depends heavily on the potential as well which has been observed in the differences between Figure 4.1 and 4.2a. To obtain a complete picture of the temperature effect, we have made a 2D map of the FE for CO as a function of potential and temperature, as we have done before for an Au rotating ring disk electrode (RRDE).¹² This is easily feasible if several potentials can be studied within a single experiment such as in a RRDE system, but requires significantly more experiments when electrolysis experiments are required such as when GC and HPLC are being used as product detection methods.

Figure 4.3a shows the effect of temperature and potential on the FE towards CO on Ag in a 2D plot. The gray dots indicate the measured datapoints and the map was constructed by interpolation between these points. It can be seen that the temperature effect is very potential dependent. At high overpotentials the temperature has a negative effect on the FE, while at low overpotentials it has a positive effect on the FE.

The difference in temperature dependence with potential might be caused by a change in reaction order of CO₂ with potential. Singh et al.³⁵ suggested that the effect of CO₂ bulk concentration is stronger at higher overpotentials because of an increase of the adsorption free energy of CO₂ with higher overpotentials, which increases the reaction order. Zhu et al.³⁶ also indicate a dependence of the reaction order in CO₂ with potential. They attribute this to differences in adsorbates on the surface. However, we measured the reaction order at different potentials and do not observe the same trend (Figure C.6). At high overpotentials, as used in both references, the reaction order might increase.

However, at lower overpotentials we observe a reaction order which is even higher than at these high overpotentials. Moreover, the reaction orders at high overpotentials in our experiments are significantly lower than observed by both references.^{35,36} We have observed before that on Au the effect of temperature is stronger at lower overpotentials. As a stronger dependence on the CO₂ concentration with increasing overpotential has not been observed, this is most likely due to the activation barrier becoming smaller with larger overpotentials as expressed in equation 4.4, where ΔH^\ddagger is the activation enthalpy, ΔH_0^\ddagger is the

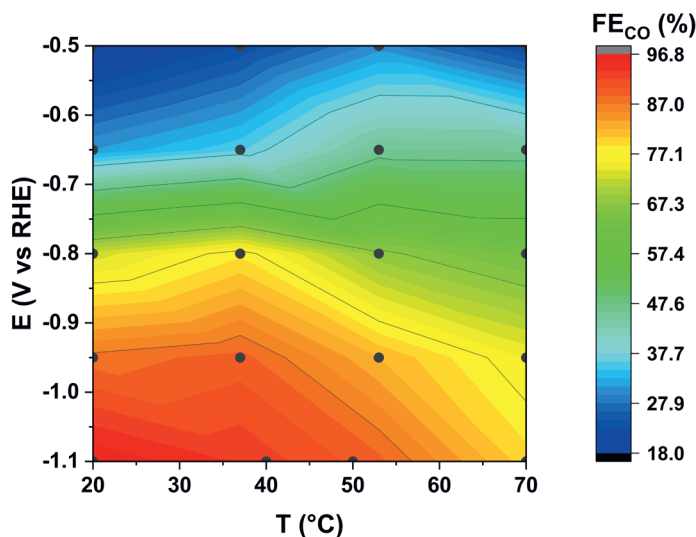


Figure 4.3 FE towards CO vs temperature and potential on Ag in 0.1 M KHCO_3

activation enthalpy at the standard equilibrium potential, α_H is the enthalpic transfer coefficient, F is the Faraday constant and η the overpotential:³⁷⁻³⁹

$$\Delta H^\ddagger = \Delta H_0^\ddagger + \alpha_H F \eta \quad (4.4)$$

The FE map with potential and temperature of Ag differs significantly from the map of Au observed before.¹² In that study, the magnitude of the temperature effect differed with potential, but it always showed a positive effect of temperature on the FE up to 55 °C, independently of potential. However, in the case of Au, the measurements were performed with an RRDE setup, while in this study on Ag, the measurements were performed in an H-cell configuration. To check if this difference in setup and measuring method causes the differences in the temperature-potential map or if this is caused by the differences in catalyst material, we have performed experiments with Au in the H-cell setup as well. Figure C.7 shows similar results as on Ag, namely a decreasing efficiency with temperature.

This indicates that the temperature effect will differ between different setups. In the RRDE setup used before, rotation rates of 2500 rpm were used to create a controlled convection in the cell, which results in higher mass transport than in the H-cell.⁴⁰ So in the H-cell, mass transport might be limiting, as observed before in literature.³ However, we observe that the current for CO₂RR stays stable at -0.80 V vs RHE on the Au with increasing temperature, but with increasing potential the

4. The temperature dependence of electrochemical CO₂ reduction on Ag and CuAg alloys

current can still increase, which would not be possible if the system is mass transport limited. However, the local environment has shown to be important for the activity of CO₂RR and this environment can be different due to differences in mass transport.^{36,41–43} Mass transport is likely to already show an effect before mass transport limited currents are reached,^{43,44} for example by influencing the local CO₂ concentration, which influences the rate as seen by the reaction order measurements, or by influencing the local pH.⁴⁵

To check if the observed differences are due to differences in mass transport and to observe the effect of mass transport on the Ag electrode, we have increased the CO₂ flow through the H-cell. Experiments in the RRDE setup as discussed above for Au are much less straightforward for Ag, also because the latter electrode material produces significant amounts of formate. Figure C.8 illustrates that higher flow rates lead to a higher limiting current for the ferricyanide couple, showing an improved mass transport at higher flows.⁴⁴ Figure C.9 shows that mass transport does influence the Faradaic efficiencies for CO₂ reduction on Ag, but not as expected. At high overpotential of -1.1 V vs RHE, the CO₂ current density increases with increased flow rate, but the H₂ current density increases as well, leading to a similar Faradaic efficiencies. At a lower overpotential of -0.8 V vs RHE, the FE increases with temperature at the higher flow rates. Interestingly, it is not that CO₂ is mass transport limited at these potentials as enhanced mass transport actually decreased the FE towards CO at low temperatures. This is because better mass transport enhances HER instead of CO₂RR and this effect seems larger at lower temperatures. Lower HER with lower mass transport has been observed previously on Au,⁴⁶ although in an RRDE system the opposite has also been observed.⁴⁷ Clark et al.^{48,49} show that at high overpotentials increased flow rates decrease HER, but for the currents at low overpotentials this trend seems opposite.⁴⁹ How the HER during CO₂RR exactly depends on mass transport is an interesting matter on its own, but outside the scope of this paper. These results show that with increased mass transport conditions, similar results as previously for Au¹² can be obtained, where increasing temperature increases the FE towards CO up to about 50 °C. This illustrates that mass transport is important in determining the temperature dependence, but also that the effect of temperature with mass transport might not be intuitive and depends on potential as well. To fully understand the interdependence between mass transport and temperature and its effect on HER and CO₂RR, more study is required into this complex issue.

The local environment might not only be different due to the differences in mass transport between the RRDE and H-cell experiments, but also due to the electrochemical measurement technique. For this study chronoamperometry (CA) has been used, while for the previous study a linear sweep voltammogram (LSV)

was taken. During a LSV the system might not be in steady state,⁴⁹⁻⁵¹ especially the local pH and CO₂ concentration might be very different than during an CA. As we see a clear dependence of the CO₂RR on both Ag and Au¹² on the CO₂ concentration, this might partially explain the differences observed.

4.3.2 Temperature effect on CuAg alloys

We have shown previously that on Cu, HER starts to dominate at elevated temperatures. Moreover, we have shown that the effect of temperature leads to an optimum in CO₂RR activity and C₂+ selectivity around 48 °C. At higher temperatures only little CO₂RR takes place, of which most results in CO.¹⁴ Alloying Ag with Cu has been shown before to result in more C₂+ products, and specifically more oxygenates such as ethanol and acetate.^{15,19,21} Studying the effect of CuAg surface alloys can be interesting to probe the effect of temperature on these minor products, which are difficult to detect on a Cu catalyst. To enhance the production of minor products even more, CsHCO₃ is used as electrolyte as it has shown to enhance the production of multicarbon products on Cu.^{52,53} Moreover, we have

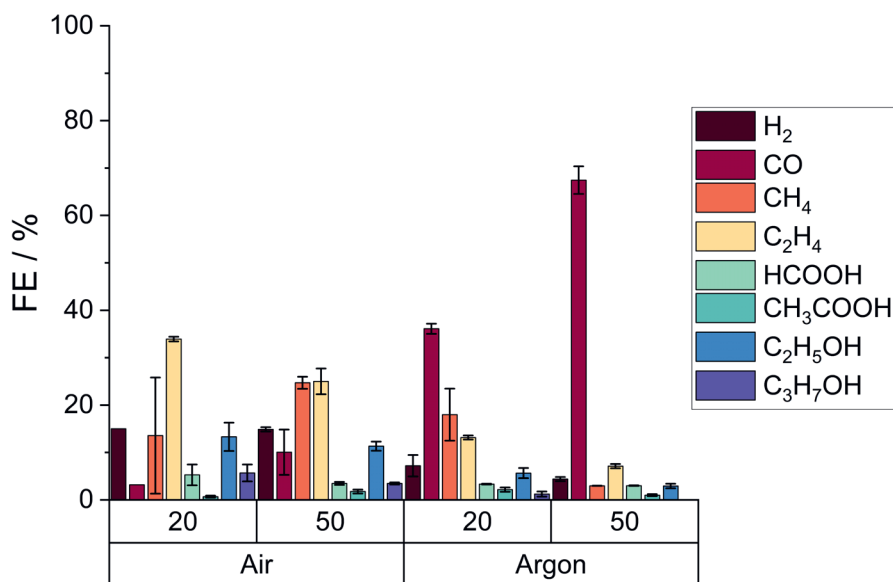


Figure 4.4 The effect of the galvanic exchange procedure on the Faradaic efficiencies of the CuAg alloys at room temperature at -1.1 V vs RHE in 0.1 M CsHCO₃. Both the concentration of AgNO₃ and the nature of the gas atmosphere influences the galvanic exchange leading to differences in FE.

4. The temperature dependence of electrochemical CO₂ reduction on Ag and CuAg alloys

shown above that Ag generates less H₂ at high temperatures and it might be able to prevent the dominance of HER on Cu at 70 °C, for example by stabilizing the copper structure via strain effects.²¹The CuAg surface alloys have been synthesized via a galvanic exchange procedure. Figure 4.4 shows that both the AgNO₃ concentration and the gas composition during galvanic exchange have effect on the product distribution of the formed CuAg surface alloy. These differences in product distribution might be related to differences in morphology and Ag content caused by the different conditions during galvanic exchange. We determined the electrochemical surface area (ECSA) by measuring the double layer capacitance as a measure of the morphology. Figure C.10 shows that the ECSAs are very similar between the different samples and do not explain the trends observed. With XPS, the Ag content near the surface was determined, as shown in Figure C.11 and Table C.1. The XPS results relate very well to the activity trends observed in Figure 4.4, where more Ag leads to more CO and less ethylene selectivity. As expected, samples contain more Ag with more AgNO₃ in the galvanic exchange solution, but surprisingly also the gas atmosphere significantly influences the amount of Ag present, with an Ar atmosphere leading to more Ag in the catalyst than an air atmosphere.

We decided to continue the temperature dependence experiments with the CuAg synthesized in 20 μM AgNO₃ in air (hereafter called CuAg20) as this produces the most C₂⁺ products and oxygenates, and the CuAg produced in 50 μM AgNO₃ in argon (hereafter called CuAg50) as this catalyst produces the least amount of H₂. Figure C.12 shows the SEM images of these two catalysts. These images show that the overall structure of the catalyst is not that different. Both electrodes do not show the very flat surface which was observed for Cu,¹⁴ but seem more flaky. This could be caused by the galvanic exchange at open circuit potential, which will probably oxidize the copper surface and change its morphology. The ECSA measurements in Figure C.10 show indeed that the CuAg alloys are slightly rougher than pristine Cu, although the differences are not very large. EDX analysis has been performed as well to observe where the Ag is located on these CuAg surface alloys. Figure C.13 shows that in both cases the Ag is spread over the entire surface as would be expected from galvanic exchange.

Figure C.14 shows the effect of temperature on both CuAg surface alloys. The CuAg20 has a broader range of products similar to Cu whereas CuAg50 is dominated by CO. Moreover, the product distribution on the CuAg20 is more effected by temperature than on the CuAg50. The latter is hardly influenced by the temperature, while the first has a similar behaviour as bare Cu. To compare the different catalysts better with each other and with bare Cu, we have plotted

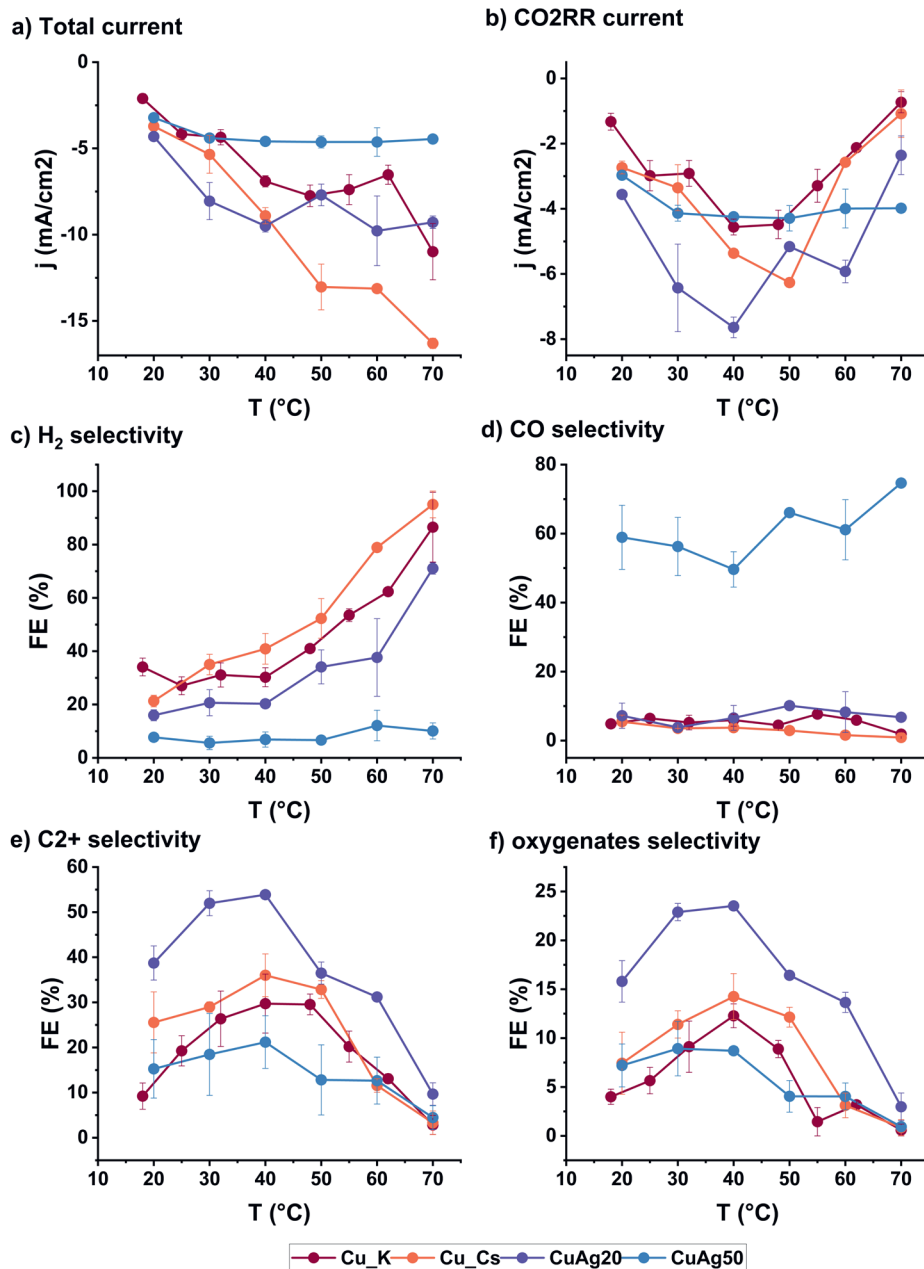


Figure 4.5 a) Total current density and b) current density towards CO₂RR and faradaic efficiency for c) hydrogen d) CO e) C₂+ products f) oxygenates for Cu, CuAg₂₀ and CuAg₅₀ at -1.1V vs RHE in 0.1 M CsHCO₃ and also in 0.1 M KHCO₃ for Cu.¹⁴

4. The temperature dependence of electrochemical CO₂ reduction on Ag and CuAg alloys

them together in Figures 4.5, C.16 and C.17. Here we also compare the data of pure Cu in CsHCO₃ with the data obtained previously in KHCO₃.¹⁴ At room temperatures, the Cs⁺ containing electrolyte results in less hydrogen and more C₂⁺ products than the K⁺ electrolytes, as expected from literature.^{52,53} However, with increasing temperature the difference between the two electrolytes becomes less pronounced and at the higher temperatures the K⁺ containing electrolytes produce less hydrogen, as shown in Figure 4.5b and C.12f. This indicates that the cation identity might be an important parameter for the stability of Cu at elevated temperatures and to inhibit HER at elevated temperatures. For the CuAg alloys, the cation does not have a significant effect on the HER selectivity, but it changes the CO₂RR product distribution from more CH₄ in K⁺ containing electrolytes to more C₂⁺ products in Cs⁺ containing electrolytes, as shown in Figure C.15.

4 It can be seen in Figure 4.5 that although the selectivities are different among the catalysts, most trends on the CuAg alloys resemble the trends with temperature on the bare Cu electrode, especially for the CuAg₂₀. Interestingly, the total current density and in particular the CO₂RR current density of the CuAg₅₀ is very stable with temperature, whereas the Cu and CuAg₂₀ show an increase in total current density and an optimum in CO₂RR current density. The CuAg₅₀ resembles more the Ag catalyst shown in Figure 4.1, as it also produces significantly higher amounts of CO than the other catalysts. Remarkably, it shows a very stable HER selectivity with temperature, while the CuAg₂₀ follows the trend of Cu, although both the activity and selectivity towards H₂ are significantly lower than on pure Cu, even compared to the pure Cu in KHCO₃ electrolyte. This indicates that the dominance of HER at elevated temperatures can be suppressed by alloying the Cu with Ag. Alloying might stabilize Cu, which would also explain why we observe almost no cation effect on the HER on the CuAg electrode, whereas there is a clear cation effect on Cu. The increased HER in Cs⁺ containing electrolytes on Cu could be due to the instability of the Cu at elevated temperatures; by stabilizing the Cu with Ag this effect appears to be eliminated.

Both CuAg alloys show an optimum in C₂⁺ products. Interestingly, on the CuAg₅₀, where the CO coverage on Cu sites is likely to be high due to the large amount of CO produced, the optimum is the least pronounced. The increase in C₂⁺ products with temperature up to 40 °C is the least for this catalyst, indicating that CO coverage is probably important for the increasing C₂⁺ selectivity in the first regime. However, even when CO is produced significantly on the CuAg₅₀, at high temperature C₂⁺ activity still decreases. Moreover, Figure C.16 shows that the effect of temperature on most carbon efficiencies is relatively stable for the CuAg₂₀ compared to the pure Cu. This seems mostly due to the higher C₂⁺ and lower formic

acid production at lower temperatures for the CuAg20 compared to the pure Cu catalyst.

CuAg20 also produces relatively large amounts of minor liquid products, which makes it possible to observe the temperature effect on acetate, 1-propanol, propionaldehyde and acetaldehyde in more detail (Figure 4.6). Interestingly, the CE of acetate increases with temperature. From all other products, this is only the case for CO. This might indicate that acetate follows a different mechanism than the other C2+ products.⁵⁴ It has recently been suggested that a ketene intermediate has to desorb from the catalyst surface which then forms acetate in solution by reacting with OH.⁵⁵ Similarly to CO, desorption would be important to form this product and can be facilitated by increasing temperatures, leading to increased CE for both CO and acetate. Acetaldehyde is another stable intermediate for which we can expect desorption to be important to obtain higher efficiencies. However, we do not observe a continuous increase in CE with temperature for acetaldehyde. Similar to

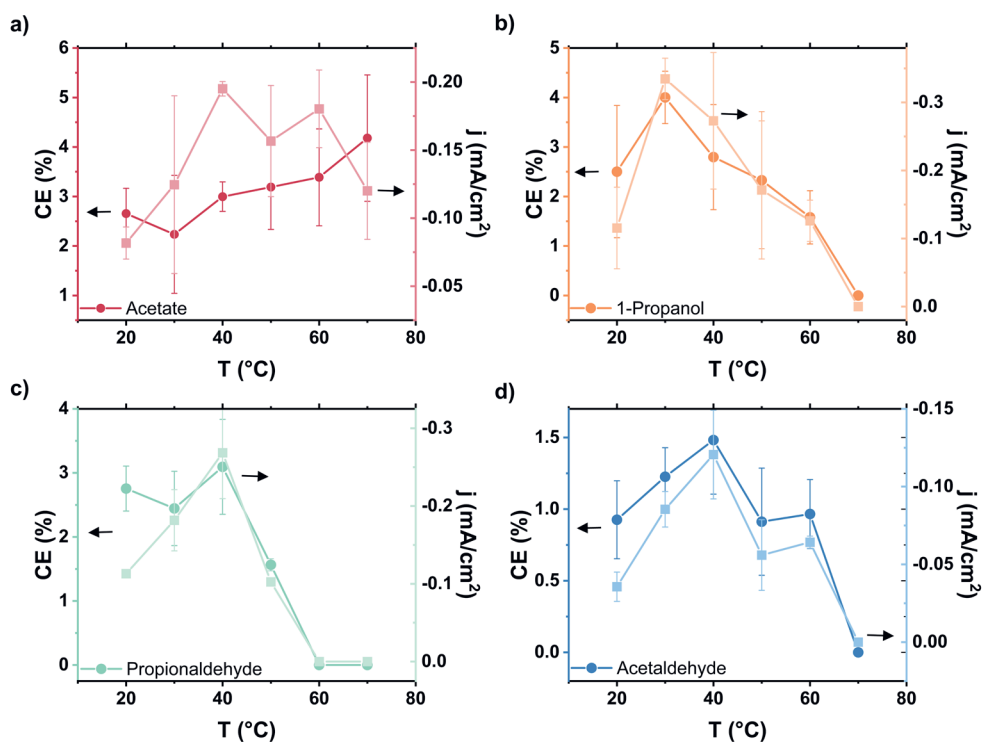


Figure 4.6 Carbon efficiency and partial current density for minor liquid products on CuAg20 at -1.1 V vs RHE in CsHCO₃ a) acetate b) 1- propanol c) propionaldehyde and d) acetaldehyde. All data has been corrected for the evaporation of the liquid products as described in the SI

the other minor products 1-propanol and propionaldehyde, it shows an optimum in CE and partial current density with temperature and an optimal production is obtained around 30-40 °C.

These results show that alloying Cu, in this case with Ag, can be an effective strategy to counteract the negative impact of temperature at temperatures above 50 °C, where hydrogen starts to dominate at Cu. With the proper alloy, it seems possible to inhibit the HER, even at temperatures up to 70 °C. However, the decrease in C₂+ products at elevated temperatures seems more intrinsic and has been observed not only for pure Cu, but also for the different CuAg alloys studied. Thus, depending on the desired product, the proper temperature and alloy should be chosen carefully. For C₂+ products, often desired when Cu is used as catalyst, the optimum temperature remains around 40-50 °C.

4.4 Conclusion

In this chapter we have shown that the activity of Ag for CO₂ reduction to CO is almost temperature independent at -1.1 V vs RHE. We show that this is due to the interplay of potential, CO₂ concentration and mass transport on the temperature effect on CO₂RR. It is important to deconvolute these effects to obtain better insight in the intrinsic effect of temperature. The intrinsic kinetics of CO₂RR on Ag seems to favour higher temperatures, also compared to HER. However, the strong dependence on the bulk concentration counteracts this effect and results in a very moderate overall temperature effect. Increased mass transport can lower CO₂RR selectivity by increasing HER activity. However, the exact effect of (temperature on) mass transport on the CO₂RR and the competing HER is not fully understood and would require more detailed study. Therefore, it would be interesting to complement studies in H-cell configurations with other setups such as rotating ring disk setups and gas diffusion electrode configurations. Moreover, the effect of temperature can be potential dependent, so to fully understand this effect, one can not suffice with measuring the temperature effect at a single potential. Instead, the interplay between potential and temperature should be investigated by studying at least two different parameters, as illustrated by the 2D map of the effect of potential and temperature on selectivity.

Surface alloying of Ag on Cu can alter the effect of temperature on the CO₂ reduction of Cu. However, it does not alter the temperature dependence of C₂+ products at high temperatures. In all cases an optimum at 40-50 °C has been observed and at higher temperatures both activity and selectivity towards C₂+ products such as ethylene and ethanol decreases. Acetate seems to be an exception as its carbon efficiency keeps increasing with increasing temperature. More importantly, the dominance of HER seems to be cation dependent on pure Cu and

could be reduced with the CuAg20 catalysts and even be removed completely with the CuAg50 catalyst. This indicates that alloying might be able to give more robust Cu based catalysts at higher temperature, although significant development is still required to attain the Cu alloy with the desired properties and selectivities at elevated temperatures.

References

1. De Luna, P. *et al. Science* **364**, eaav3506 (2019).
2. Mikkelsen, M., Jørgensen, M. & Krebs, F. C. *Energy and Environmental Science* vol. 3 43–81 (2010).
3. Hatsukade, T., Kuhl, K. P., Cave, E. R., Abram, D. N. & Jaramillo, T. F. *Physical Chemistry Chemical Physics* **16**, 13814–13819 (2014).
4. Hansen, H. A., Varley, J. B., Peterson, A. A. & Nørskov, J. K. *Journal of Physical Chemistry Letters* **4**, 388–392 (2013).
5. Lu, Q. *et al. Nat Commun* **5**, (2014).
6. Kibria, M. G. *et al. Advanced Materials* **31** (2019).
7. Feaster, J. T. *et al. ACS Catal* **7**, 4822–4827 (2017).
8. Sun, D., Xu, X., Qin, Y., Jiang, S. P. & Shao, Z. *ChemSusChem* vol. 13 39–58 (2020).
9. Bagger, A., Ju, W., Varela, A. S., Strasser, P. & Rossmeisl, J. *ChemPhysChem* **18**, 3266–3273 (2017).
10. Rosen, J. *et al. ACS Catal* **5**, 4293–4299 (2015).
11. Raaijman, S. J., Schellekens, M. P., Corbett, P. J. & Koper, M. T. M. *Angewandte Chemie - International Edition* **60**, 21732–21736 (2021).
12. Vos, R. E. & Koper, M. T. M. *ChemElectroChem* **9**, e20220023 (2022).
13. Dufek, E. J., Lister, T. E. & McIlwain, M. E. *J Appl Electrochem* **41**, 623–631 (2011).
14. Vos, R. E. *et al. ACS Catal* **13**, 8080–8091 (2023).
15. Wang, L. *et al.* **117**, (2020).
16. Wei, D. *et al. Angewandte Chemie - International Edition* **62**, (2023).
17. Hailu, A. & Shaw, S. K. *J Electrochem Soc* **167**, 126509 (2020).
18. Choi, C. *et al. Nano Res* **14**, 3497–3501 (2021).
19. Robens, E., Hecker, B., Kungl, H., Tempel, H. & Eichel, R. A. *ACS Appl Energy Mater* **6**, 7571–7577 (2023).
20. Xu, Y. *et al. ACS Appl Mater Interfaces* **14**, 11567–11574 (2022).
21. Clark, E. L., Hahn, C., Jaramillo, T. F. & Bell, A. T. *J Am Chem Soc* **139**, 15848–15857 (2017).
22. Lee, S., Park, G. & Lee, J. *ACS Catal* **7**, 8594–8604 (2017).
23. Iyengar, P., Kolb, M. J., Pankhurst, J. R., Calle-Vallejo, F. & Buonsanti, R. *ACS Catal* **11**, 4456–4463 (2021).
24. Gao, J. *et al. J Am Chem Soc* **141**, 18704–18714 (2019).
25. Ting, L. R. L. *et al. ACS Catal* **10**, 4059–4069 (2020).
26. Jeon, Y. E. *et al. Journal of Industrial and Engineering Chemistry* **116**, 191–198 (2022).
27. Chang, C.-J. *et al. J Am Chem Soc* **142**, 12119–12132 (2020).
28. Li, Y. C. *et al. J Am Chem Soc* **141**, 8584–8591 (2019).
29. Wuttig, A. & Surendranath, Y. *ACS Catal* **5**, 4479–4484 (2015).
30. Plummer, L. N. & Busenberg, E. *Geochim Cosmochim Acta* **46**, 1011–1040 (1982).
31. Morales, D. M. & Risch, M. *Journal of Physics: Energy* **3**, 34013 (2021).
32. Strohmeier, B. R. *Journal of Vacuum Science & Technology A* **14**, 481–484 (1996).
33. Shard, A. G. *Journal of Vacuum Science & Technology A* **38**, 041201 (2020).

34. Vos, R. E. & Koper, M. T. M. *ACS Catal* 4432–4440 (2024)
doi:10.1021/acscatal.4c00009.
35. Singh, M. R., Goodpaster, J. D., Weber, A. Z., Head-Gordon, M. & Bell, A. T. *Proc Natl Acad Sci U S A* **114**, E8812–E8821 (2017).
36. Zhu, X., Huang, J. & Eikerling, M. *ACS Catal* **11**, 14521–14532 (2021).
37. Gojković, S., Zečević, S. & Dra, D. *Journal of Electroanalytical Chemistry* vol. 399 (1995).
38. Conway, B. E. & Wilkinsont, D. P. *J. Chem. SOC., Faraday Trans. I* vol. 85 (1989).
39. Protsenko, V. S. & Danilov, F. I. *Journal of Electroanalytical Chemistry* **651**, 105–110 (2011).
40. Marcandalli, G., Goyal, A. & Koper, M. T. M. *ACS Catal* 4936–4945 (2021)
doi:10.1021/acscatal.1c00272.
41. Bui, J. C. *et al. Acc Chem Res* **55**, 484–494 (2022).
42. Zhang, Q. *et al. Adv Funct Mater* **31**, (2021).
43. Dolmanan, S. Bin *et al. J Mater Chem A Mater* **11**, 13493–13501 (2023).
44. Qi, Z., Hawks, S. A., Horwood, C., Biener, J. & Biener, M. M. *Mater Adv* **3**, 381–388 (2022).
45. Marcandalli, G., Monteiro, M. C. O., Goyal, A. & Koper, M. T. M. *Acc Chem Res* **55**, 1900–1911 (2022).
46. Zhang, B. A., Ozel, T., Elias, J. S., Costentin, C. & Nocera, D. G. *ACS Cent Sci* **5**, 1097–1105 (2019).
47. Goyal, A., Marcandalli, G., Mints, V. A. & Koper, M. T. M. *J Am Chem Soc* **142**, 4154–4161 (2020).
48. Clark, E. L. *et al. ACS Catal* **8**, 6560–6570 (2018).
49. Clark, E. L. & Bell, A. T. *J Am Chem Soc* **140**, 7012–7020 (2018).
50. Anantharaj, S., Kundu, S. & Noda, S. *J Electrochem Soc* **169**, 014508 (2022).
51. Marcandalli, G., Villalba, M. & Koper, M. T. M. *Langmuir* **37**, 5707–5716 (2021).
52. Ringe, S. *et al. Energy Environ Sci* **12**, 3001–3014 (2019).
53. Resasco, J. *et al. J Am Chem Soc* **139**, 11277–11287 (2017).
54. Wang, H. *et al. Curr Opin Electrochem* **39**, (2023).
55. Heenen, H. H. *et al. Energy Environ Sci* **15**, 3978–3990 (2022).